Journal of Medicinal Chemistry

Article

Discovery of a Selective and Potent Inhibitor of Mitogen-Activated Protein Kinase-Interacting Kinases 1 and 2 (MNK1/2) Utilizing Structure-Based Drug Design

Wooseok Han, Yu Ding, Yongjin Xu, Keith Pfister, Shejin Zhu, Robert Warne, Mike Doyle, Mina Aikawa, Payman Amiri, Brent Appleton, Stuart D. Darrin, Abdallah Fanidi, and Cynthia M. Shafer

J. Med. Chem., **Just Accepted Manuscript** • DOI: 10.1021/acs.jmedchem.5b01657 • Publication Date (Web): 22 Mar 2016

ACS Publications

Journal of Medicinal Chemistry is published by the American Chemical Society. 1155 Sixteenth Street N.W., Washington, DC 20036

Discovery of a Selective and Potent Inhibitor of Mitogen-Activated Protein Kinase-Interacting Kinases 1 and 2 (MNK1/2) Utilizing Structure-Based Drug Design

Wooseok Han[χ], Yu Ding[χ], Yongjin Xu[χ], Keith Pfister[χ], Shejin Zhu[χ], Bob Warne[ξ], Mike Doyle[ξ], Mina Aikawa[ξ], Payman Amiri[ξ], Brent Appleton[χ], Darrin D. Stuart[ξ], Abdallah Fanidi[ξ], Cynthia M. Shafer[χ]*

[χ]Global Discovery Chemistry, Novartis Institutes for BioMedical Research, 4560 Horton Street, Emeryville, CA 94608

[ξ]Oncology, Novartis Institutes for BioMedical Research, 4560 Horton Street, Emeryville, CA 94608

KEYWORDS. mitogen-activated protein kinase-interacting kinase, MNK, EIF4E, protein kinase, cancer, oncology, small molecule inhibitor, structure-based drug design.

ABSTRACT. The discovery of a highly potent and selective small molecule inhibitor **9** for in vitro target validation of MNK1/2 kinases is described. The aminopyrazine benzimidazole series

was derived from an HTS hit and optimized by utilization of a docking model, conformation analysis, and binding pocket comparison against anti-targets.

INTRODUCTION

Mitogen-activated protein (MAP) kinase-interacting kinases 1 and 2 (MNK1/2) are serine/threonine protein kinases that phylogenetically belong to the group of Ca^{2+}/calmodulin-dependent kinases (CaMK). Each MNK gene, *MKNK1* and *MKNK2*, produce two alternatively spliced isoforms, encoding MNK1a, MNK1b, MNK2a and MNK2b proteins. MNK1a/2a contain a MAPK-binding site in the C-terminal regions, which can be activated through phosphorylation by ERK and p38 MAPK, while the 'b' isoforms are constitutively active and lack this MAPK-binding site.[1,2]

In tumor cells, aberrant regulation of MAPK signaling pathways[3] leads to uncontrolled cell division, invasiveness, survival and underlying these cancer phenotypes is dysregulated cell metabolism and protein synthesis.[4] Protein synthesis is tightly controlled through regulation of mRNA translation and a key player in this process is the eukaryotic initiation factor 4F (eIF4F) which is a cap-binding complex that binds the 5′ 7-methyl guanosine cap found on all cellular mRNAs. It is comprised of eukaryotic initiation factor E (EIF4E), the DEAD-box helicase, eukaryotic initiation factor 4A (EIF4A), and the scaffold protein eukaryotic initiation factor 4G (EIF4G).[5] Among them, the cap-binding protein EIF4E is the limiting factor for the assembly of the eIF4F complex[6,7] and acts as a convergence point for RAS-RAF-MEK-ERK and PI3K-AKT-mTOR pathways.[8] Phosphorylation of EIF4E occurs at a single site, S209, which is mediated by MNK1/2 kinases.[9] High levels of phospho-EIF4E are found in various types of cancers and several studies demonstrate that MNK1/2-mediated phosphorylation is essential for EIF4E's role in oncogenic transformation.[10–12]

For example, genetic studies using mouse models clearly demonstrate an oncogenic role for Mnk1/2 mediated phosphorylation of Eif4e in an *Eμ-Myc* mouse lymphoma model.[13] In this model, wild-type Eif4e and a phospho-mimetic mutant, Eif4e (S209D) cooperated with Myc in accelerating lymphomagenesis, whereas a phospho-defective mutant Eif4e (S209A) did not. A direct role for Mnk1-mediated phosphorylation was demonstrated by transfecting hematopoietic stem cells from these mice with a kinase-defective Mnk1 mutant (T2A2) or a constitutively active mutant (T332D). While the active mutant readily formed tumors, the kinase-defective mutant did not. Additional evidence for Mnk1/2 in mouse tumorigenesis comes from *Ras* and $Pten^{-/-}$ genetically engineered mouse models.[14,15]

There is also evidence that MNK1/2 could play a role in human tumor cells.[11] Feedback activation of MNK1/2 in response to targeted therapies such as imatinib[16], rapamycin and other rapalogs[17–20] or chemotherapies such as cytarabine[21] results in increased phosphorylation of EIF4E which potentially diminishes the therapeutic activity. Inhibition of MNK1/2 in combination with these therapies enhanced the antitumor activity. Simultaneous inhibition of MNK1/2 and Bruton's tyrosine kinase (BTK) or androgen receptor (AR) as a dual inhibitor enhanced antiproliferative activity against activated diffuse large B-cell lymphoma (DLBCL) cell lines or AR sensitive prostate cancer cell lines compared to a single agent treatment.[22–24] Taken together, these data support a role for MNK1/2-mediated phosphorylation of EIF4E in oncogenesis and cancer therapeutic resistance.[11,12]

While other MNK1/2 substrates such as SPRY2,[25,26] PSF,[27] hnRNP A1,[28] and cPLA2[29] could play a role in tumorigenesis,[12] the most compelling evidence supports a critical role of EIF4E.[30] In contrast to their role in tumorigenesis, MNK1/2 appear to be dispensable for normal

development in mouse knock-out studies[31] and this potential difference may provide a therapeutic avenue for targeting translational requirements in cancer.[11,32,33]

Several MNK inhibitors such as N^3-(4-fluorophenyl)-1*H*-pyrazolo[3,4-*d*]pyrimidine-3,4-diamine (**1**, CGP57380) and cercosporamide have been widely described in literature.[11,34–36] **1**, which was first identified by Novartis,[37] is a weak inhibitor of MNK1/2 with low micromolar IC_{50} values and exhibits poor selectivity against other kinases.[12,38,39] While cercosporamide is more potent in in vitro assays and shows antitumor efficacy in mouse xenograft models,[40,41] it inhibits JAK3 and PKCβ with submicromolar activites.[42] Therefore, we undertook to develop more potent and selective MNK1/2 inhibitors that could be used to better understand the consequences of MNK1/2 inhibition in cancer. Herein, we describe the discovery of a selective and potent inhibitor of MNK1/2 kinases via a structure-based drug design approach.

Figure 1. (a) Co-cyrstal structure of staurosporine in a mutated MNK2 (2HW7); (b) Overlay model of compound **2** on staurosporine in a mutated MNK2.

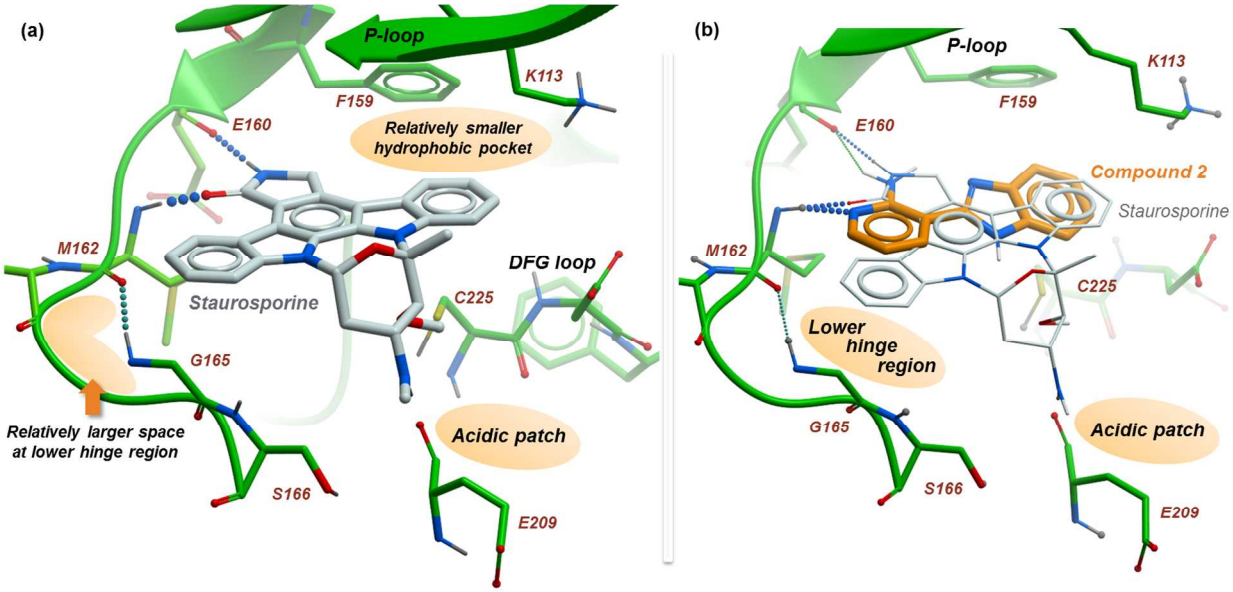

RESULTS AND DISCUSSION

Since dual inhibition of MNK1 and MNK2 kinases was desired to maximize antitumor activity, the homology of the two MNK homologs was evaluated. The amino acid sequence identity of the catalytic domain of the two isoforms was found to be 72−78%, with the ATP binding sites being even higher (90%) with only two residues out of 21 being different.[9,11] The two residues, M162L and R97K, point away from the pocket and were not expected to affect the shape of the pocket. Therefore, it was anticipated that an inhibitor in the active site could inhibit both MNK1 and NMK2 kinases with similar potencies. The catalytic domain was also compared with that of 17 other closely-related kinases[43] mostly in the Ca^{2+}/calmodulin-dependent kinase (CaMK) group. This effort indicated that MNK2 had significant sequence identity (>30%) with the catalytic domain of each of these kinases which was of concern for our ability to design selective MNK inhibitors.

With the goal of dual inhibition of MNK1 and MNK2 kinases, an HTS campaign was carried out to identify starting points for our medicinal chemistry efforts. A number of chemotypes with single digit micromolar and submicromolar MNK1/2 activity and good ligand efficiency (LE)[44] of 0.33−0.41 were identified. The hits were then docked in a co-crystal structure of staurosporine in MNK2 (Figure 1a, 2HW7) where the DFD motif on the activation loop was mutated to DFG to relieve auto-inhibition.[45] Beside the unique DFD motif, MNK kinases have a unique combination of F159 gatekeeper and C225 secondary gatekeeper, which results in a small hydrophobic pocket near the gatekeeper F159. Additionally, due to a hydrogen bond between M162 and G165, a C-shaped loop is formed near lower hinge region producing a larger cavity than in many kinases.

One of the hits identified from the HTS, a fragment-like aminopyridine benzimidazole **2**, showed submicromolar potency in biochemical assays of MNK1 and MNK2 and a high ligand efficiency (LE) value of 0.38 for both MNK1 and MNK2 (Table 1). When **2** was docked in the aforementioned staurosporine/MNK2 co-crystal structure, two hydrogen bond interactions of the aminopyridine moiety (Figure 1b) overlapped well with the donor-acceptor motif of the lactam of staurosporine. The aryl ring of the benzimidazole is pointing toward the small hydrophobic area under the F159 gatekeeper, suggesting a T-shaped edge-to-face π-π stacking interaction.[46] The overlay model of **2** on staurosporine suggested that we could identify key interactions in the lower hinge region and the acidic region around E209 for gaining potency and selectivity (Figure 1b). Based on its ligand efficiency and proposed binding mode, compound **2** was considered as a good starting point to explore the SAR of the lower hinge and the acidic patch regions.

Table 1. SAR of benzimidazole aminopyridine series at lower hinge region.

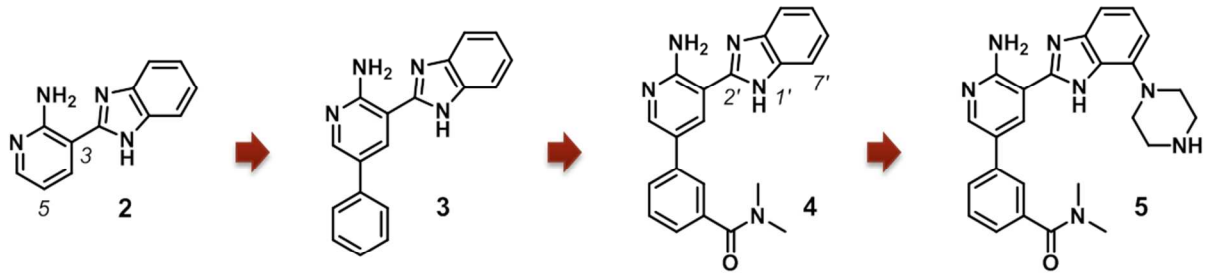

Compound	2	3	4	5
IC_{50} MNK1/2	0.70/0.90 μM	0.12/0.72 μM	0.036/0.034 μM	0.004/0.002 μM
IC_{50} CDK1/2	10/25 μM	0.16/1.3 μM	1.0/5.7 μM	1.0/4.0 μM
Sol. HT (pH 7.4)	300 μM	<0.0006 μM	<0.0003 μM	102 μM
$LogD_{7.4}$	3.0	>4.2	4.2	1.8
LipE (MNK1/2)	-	3.0/2.2	5.0/5.0	6.1/6.4

The homology model indicated that an aryl or heteroaryl ring at the C5-position of **2** could make contact with lower hinge residues and be used as a handle to explore the large C-shaped lower hinge cavity (Table 1). Compound **3** exhibited improved biochemical MNK1 and MNK2 potencies, but the selectivity against two of the identified off-targets, CDK1 and CDK2, deteriorated significantly. CDK1 and CDK2 were among the CaMKII kinases identified in the sequence alignment analysis previously discussed which had significant sequence identity to MNK2. However, the docking pose of **3** in MNK2 revealed that a polar interaction with S166[47] could be made by employing a polar substituent at the meta position of the phenyl ring. It was anticipated that the selectivity against CDK1 and CDK2 would be increased because MNK2 has the unique C-shaped lower hinge conformation due to G164 insertion compared to CDK1 and CDK2. CDK2 has a D86 in the place of the S166 in the MNK2 and CDK2 binding pocket overlay (Figure 2). Due to the C-shaped conformation, the D86 in CDK2 is slightly further away from the ligand than S166 in MNK2. Also, the S166 in MNK2 should be attractive to a hydrogen bond accepting group whereas the D86 in CDK2 is likely to be repulsive due to a lone-pair repulsion. The examination of SAR on the meta position with hydrogen bond acceptor-bearing groups led to compound **4** which further improved the biochemical potency against MNK1 and MNK2 (0.036 and 0.034 μM, respectively) and improved the selectivity against CDK1 and CDK2. The docking model of **4** (Figure 2) clearly suggested that the carbonyl oxygen of the amide functionality has a hydrogen bond interaction with the backbone NH of S166. In addition, one of the amide methyl groups is anticipated to have a hydrophobic interaction with P-loop residues. The optimization in the lower hinge region not only increased potency and selectivity, but also the lipophilic efficiency (LipE)[48] by 2.0 and 2.8 units for MNK1 and MNK2. However, the solubility was not improved, as reflected in high logD value.

Figure 2. Analysis of the C-shaped lower hinge region in MNK2 and CDK2 docked with **4**.

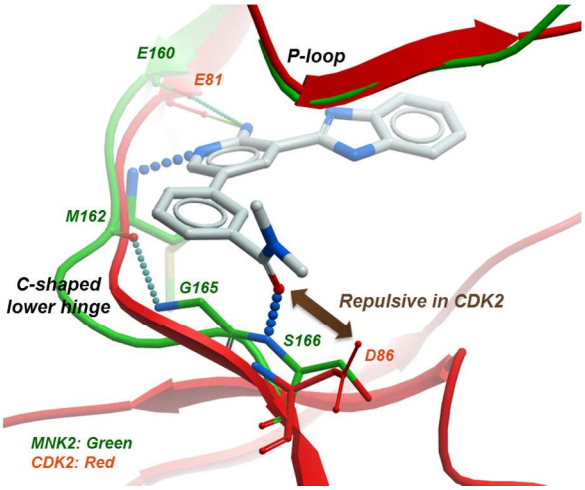

The next round of SAR examined the acidic patch region. The crystal structure and docking model suggested that the acidic patch could be reached from the 7'-position of the benzimidazole of **4** (Figure 1b). We reasoned that a basic amine-containing group would improve not only the solubility of **4** but also the MNK1 and MNK2 potencies by making hydrogen bond interactions with the glutamic acid E209 in the acidic patch. Several basic amines such as piperidine, piperazine, and aminocyclohexane were examined at the 7'-position of the benzimidazole of **4**. Compound **5** which incorporated a piperazine ring led to >10-fold increase in potency against MNK1 and MNK2 (0.004 and 0.002 μM, respectively) without loss of selectivity against CDK1 and CDK2. As anticipated, the solubility improved significantly (>100 μM), and the logD value lowered by 2.2 units. This polar interaction further improved LipE to 6.1 and 6.4 for MNK1 and MNK2, indicating that the optimization effort was progressing well.[49]

Table 2. Multi-parameter optimization of the aminopyrazine series.

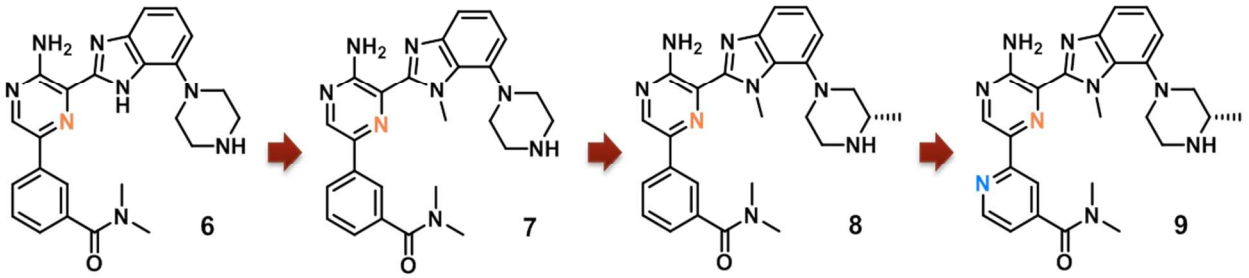

Compound		6	7	8	9
IC_{50} MNK1/2		0.08/0.02 μM	0.002/0.001 μM	0.0015/0.0007 μM	0.003/0.003 μM
EC_{50} p-EIF4E^{Ser209}		0.05 μM	0.005 μM	0.003 μM	0.0006 μM
IC_{50} CDK1/2		1.7/11 μM	0.50/1.4 μM	1.0/3.4 μM	>25/>25 μM
Sol. HT (pH 7.4)		70 μM	254 μM	201 μM	220 μM
$LogD_{7.4}$		1.9	1.1	1.7	1.9
LipE (MNK1/2)		5.0/5.6	6.7/7.0	6.3/6.6	6.9/6.9
Caco-2	P_{app}A-B	0.70 × 10^{-6} cm/s	9.0 × 10^{-6} cm/s	5.8 × 10^{-6} cm/s	5.0 × 10^{-6} cm/s
	B-A/A-B	87	2.3	2.0	5.0

Having identified a potent and selective inhibitor of MNK1 and MNK2, a mechanism-based cellular assay measuring the phosphorylation of EIF4E, a direct downstream target, of MNK1 and MNK2 was used to determine whether the biochemical inhibition of MNK1 and MNK2 kinases had an effect in a cellular context. The EC_{50} for inhibition of EIF4E phosphorylation in KMS11-luc myeloma by compound **5** was 0.13 μM.[50] While subsequent SAR examination in the aminopyridine series failed to improve cellular activity further,[51] we turned our attention to the isosteric aminopyrazine series. Although the aminopyrazines were less potent in the biochemical assays than the corresponding aminopyridine compounds, they exhibited a narrower ratio between the enzymatic and cellular readouts. For example, the aminopyrazine **6** (Table 2) was 5- to 10-fold less potent against MNK1 and MNK2 than the aminopyridine **5** (Table 1), but the cellular target modulation tracked with the biochemical potency. Because of this, the decision

was made to focus on the optimization of the aminopyrazine series with the hope of improving the biochemical potency.

To understand what was driving the difference between the enzymatic potencies of **5** and **6**, the compounds were docked in MNK2. The docking model of the more potent aminopyridine **5** indicated that the dihedral angle between the aminopyridine and benzimidazole rings was 20 degrees. The torsional energy barrier from the ground state conformation to a bioactive conformation was anticipated to be higher in the aminopyrazine **6** which has a flat conformation in the ground state due to two internal hydrogen bonds. A quantum mechanics (QM) study disclosed a ~1.4 kcal/mol of the torsional energy difference between aminopyridine and aminopyrazine benzimidazole, corresponding to 10-fold difference in potency.[52] We thought that the introduction of a methyl group on the nitrogen on the benzimidazole in **6** would disrupt the planarity, enabling **6** to attain the bioactive conformation of **5**. This change[53] did improve the biochemical potency 20- to 40-fold (0.002 and 0.001 μM for MNK1 and MNK2, respectively) as shown in **7** (Table 2). The target modulation potency of **7** also increased 10-fold to 0.005 μM. In this case, the "magic methyl" effect[54] not only influenced the biochemical potency but also the cell permeability and physicochemical properties. The removal of a hydrogen bond donor led to an increase in cell permeability (Caco-2 P_{app}A-B: 0.7×10^{-6} cm/s for **6** vs 9.0×10^{-6} cm/s for **7**), even with a decrease of logD by 0.8 units. The disruption of molecular planarity enhanced solubility 3-fold (254 μM) and drug-likeness as demonstrated in the increase of LipE value by 1.6 units.

Figure 3. Overlaying View of Van Der Waals (VDW) Surface of MNK2 and CDK2 with **7**.

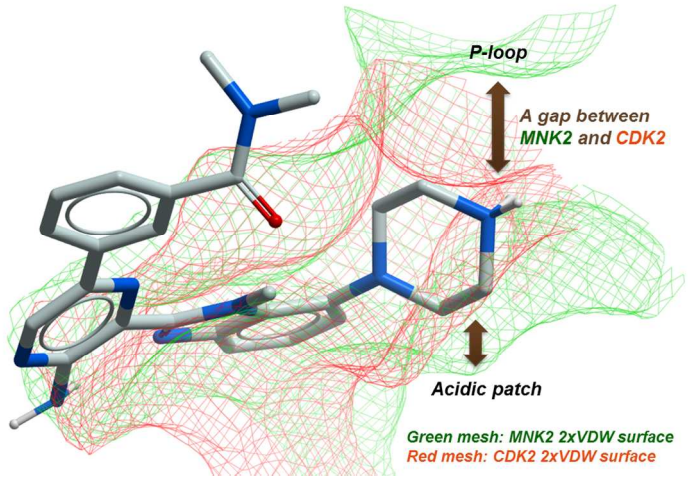

Incorporating the methyl on the benzimidazole caused the piperazine ring to become perpendicular to the plane of the benzimidazole ring. This presented the ethylene bridge of the piperazine ring to the P-loop enabling a hydrophobic interaction. The data suggest that there are differences in the P-loop regions of MNK2 and CDK2 (Table 2).[55] We therefore examined the P-loop areas in MNK2 and CDK2 by overlaying the binding pockets in order to find a difference that can be utilized to improve selectivity further. In addition to the lower hinge region as mentioned before, we found differences in both P-loop and acidic patch areas (Figure 3), where MNK2 has a different space arrangement than CDK2. It appeared from the overlay study that CDK2 might have less space in the P-loop area than MNK2. Further, the P-loop area is primarily hydrophobic. Thus, a methyl group was incorporated on the piperazine ring of **7** to provide **8** which had similar properties and biochemical potencies as **7** and improved selectivity against CDK1 and CDK2.

Finally, the lower hinge region was re-examined. Although the docking model suggested that a plausible position for the amide group should be the right-hand side of the phenyl ring to make a

hydrogen bond interaction with S166, analysis of the model suggested that the C-shaped loop between M162 and G165 at the lower hinge area is spacious enough to accommodate the amide group of **8** if it were presented on the left hand side of the phenyl ring. Thus, if the phenyl bound in a flipped binding mode which placed the amide group away from the S166 residue, the potency would be reduced due to the loss of hydrogen bond interaction. To restrict the position of the amide to the S166 residue, the phenyl ring was replaced with an ortho pyridine (**9**). Similar to a 2,2'-bipyridyl system, the rotational barrier of these two rings should be >1.5 kcal/mol based on the torsion distribution from small molecule crystal structures with the same feature.[56] This predisposes the amide group to be predominantly towards the S166 residue. While the resulting compound **9** maintained the desired potencies of MNK1 and MNK2, the activities of CDK1 and CDK2 were completely dialed out (IC_{50} >25 μM).[57]

Figure 4. Overlaying View of MNK2 and CDK2 with **9**.

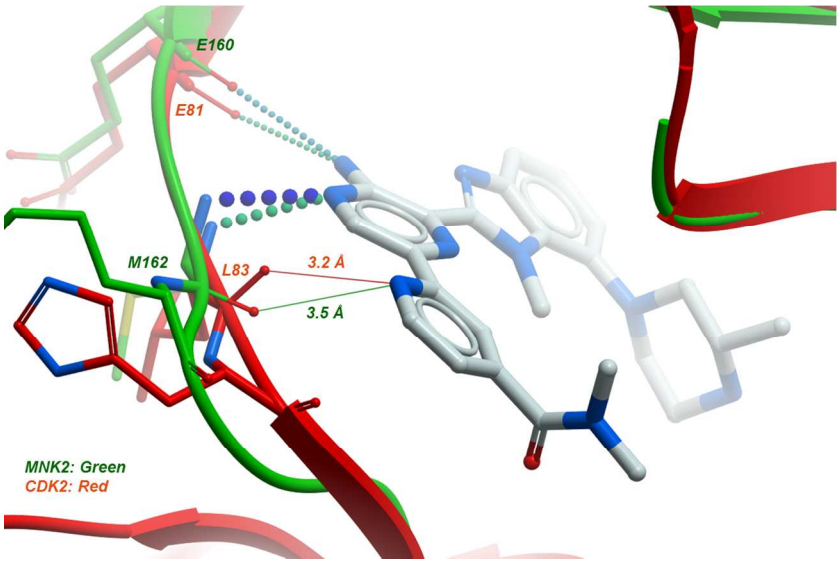

By closely analyzing the docking model of **9** in CDK2 (Figure 4), the high selectivity was found to be due to the fact that an oxygen atom of the carbonyl group on a lower hinge L83 residue of CDK2 is in closer proximity to the pyridyl nitrogen of compound **9** (3.2 Å) than that on the corresponding residue of MNK2 (3.5 Å). More importantly, the lone pair trajectories on the pyridyl nitrogen of **9** and the oxygen atom at the residue L83 in CDK2 resulted in repulsion and the high selectivity observed for CDK2. Further, compound **9** showed excellent selectivity against 53 other kinases from an internal protein kinase panel, where only four kinases were inhibited with IC_{50}'s <1 μM (CaMK2D 0.69 μM, FLT3 0.28 μM, PIM2 0.73 μM, ROCK2 0.37 μM).

While the optimization of the aminopyrazine series led to potent compounds in the p-EIF4E modulation assay, we did not collect cell proliferation data for many of the compounds in the series because the data were not informative on early compounds due to the off-target activity, including CDK1/2. We now have potent, selective compounds which exhibit moderate inhibition of cell proliferation in the KMS11-luc human multiple myeloma tumor cell line (e.g. EC_{50} for **9** = 1.7 μM)[58] and will begin exploring MNK1/2 dependency across different tumor types.

Compound **9** also exhibited good cell permeability, modest efflux in Caco-2 assay, good physicochemical properties such as solubility and logD, and the highest LipE in the aminopyrazine series. Furthermore, compound **9** did not inhibit any CYP450 isoforms (IC_{50} >40 μM) and exhibited moderate in vitro clearance in rat liver microsomes (CL_{int} 32 μL/min/mg; ER_h 0.54) suggesting that it could be used as an in vivo tool compound, although we did not investigate its behavior in vivo.

Overall, our structure-based design resulted in an enhanced kinase selectivity profile as well as >80 fold improvement in p-EIF4E EC_{50} for compound **9** compared to compound **6** (Table 2).

Based on the in vitro biochemical and target modulation potency, ADME and selectivity profile, compound **9** was selected as a lead to probe the dependence on MNK1/2 in cancer, and this is the focus of ongoing efforts.

Compound **2** was synthesized via Suzuki cross-coupling reaction of commercially available 3-(4,4,5,5-tetramethyl-1,3,2-dioxaborolan-2-yl)pyridin-2-amine and 2-bromo-1*H*-benzo[*d*]imidazole (Scheme 1). Treatment of **2** with *N*-bromosuccinimide (NBS) provided brominated intermediate **10**, which was then coupled with **11** or **12** to yield **3** or **4**. The synthesis of piperazine-containing compounds **5** and **6** started from commerically available 3-chloro-2-nitroaniline and tert-butyl piperazine-1-carboxylate, which were subjected to S_NAr amination reaction to provide nitro intermediate **13** (Scheme 2). Subsequent palladium-catalyzed hydrogenation of **13** afforded bis-anilino intermediate **14**, which was coupled with **15** or **16** to form the corresponding amide and then cyclized to give the benzimidazole intermediate of aminopyridine and aminopyrazine, **17** or **18**. Compounds **5** and **6** were obtained via Suzuki coupling reaction of boronic acid **12** with the corresponding bromo intermediate **17** or **18** followed by deprotection of Boc-group.

Scheme 1. Synthesis of compounds **2–4**.

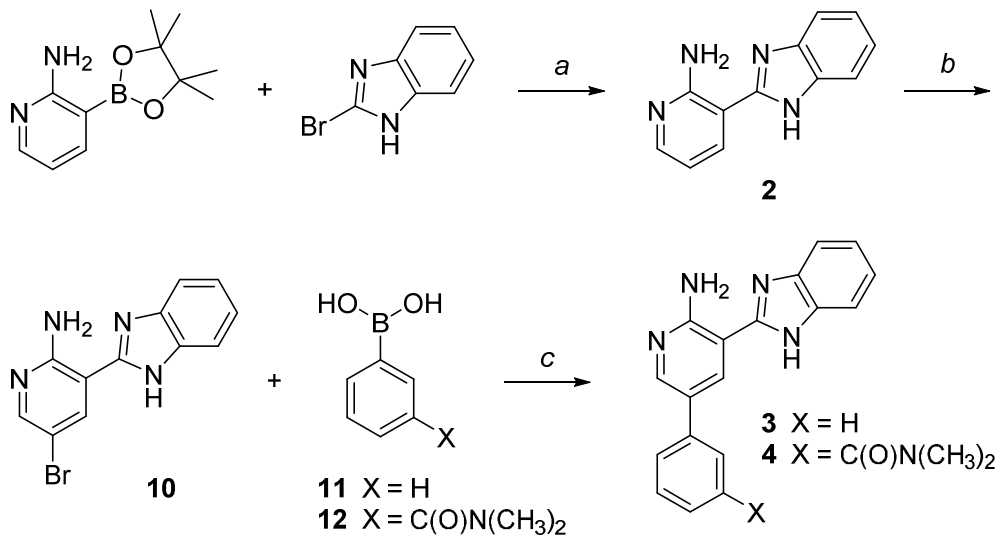

Reagents and conditions: (a) $PdCl_2(dppf)\cdot CH_2Cl_2$, DME, 2 M Na_2CO_3 (aq), 120 °C, microwave, 32%; (b) NBS, DMF, 0 °C, 20 min, 57%; (c) $PdCl_2(dppf)\cdot CH_2Cl_2$, DME, 2 M Na_2CO_3 (aq), 130 °C, microwave, 15 min, 16% for **3** and 21% for **4**.

Scheme 2. Synthesis of compounds **5** and **6**.

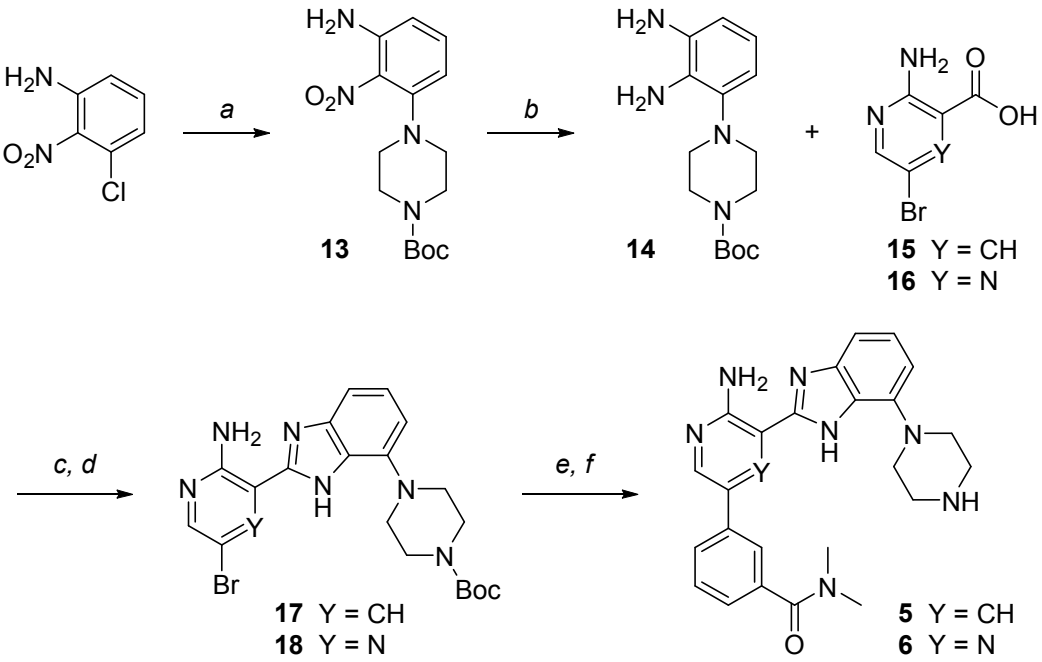

Reagents and conditions: (a) tert-Butyl piperazine-1-carboxylate, K_2CO_3, DMF, 130 °C, 28 h, 48%; (b) H_2, Pd/C, MeOH, 1 h, 96%; (c) **15** or **16**, HATU, DIEA, MeCN; (d) AcOH, 120 °C, 1

h, 41% for **17** (over 2 steps) and 35% for **18** (over 2 steps); (e) **12**, $PdCl_2(dppf)\cdot CH_2Cl_2$, DME, 2 M Na_2CO_3 (aq), 120 °C, microwave; (f) HCl in doxane, 32% for **5** (over 2 steps); TFA, CH_2Cl_2, 20% for **6** (over 2 steps).

Scheme 3. Synthesis of compounds **7**–**9**.

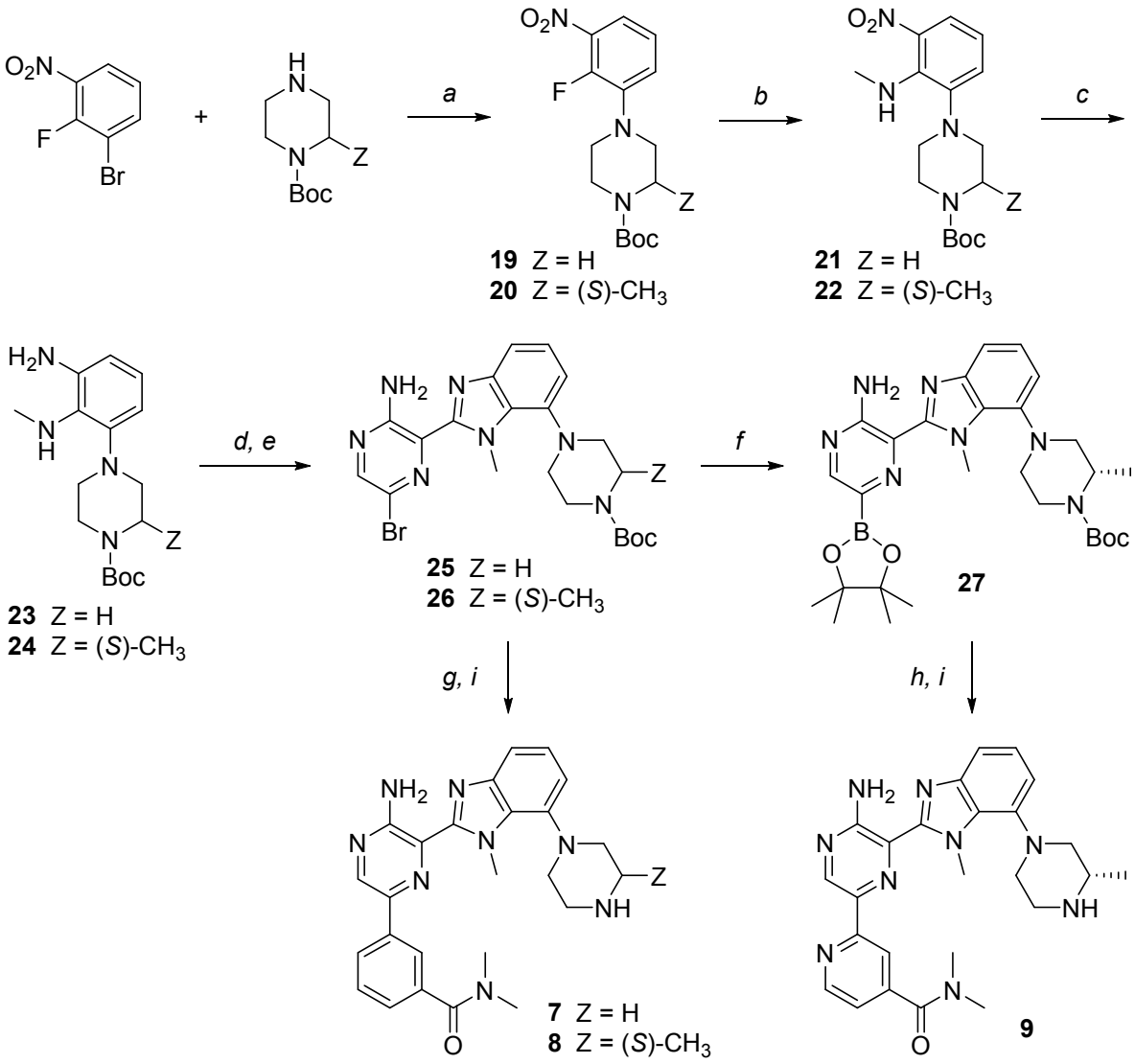

Reagents and conditions: (a) tert-Butyl piperazine-1-carboxylate or tert-butyl (*S*)-2-methylpiperazine-1-carboxylate, $Pd_2(dba)_3$, Xantphos, Cs_2CO_3, dioxane, 110 °C, 16 h, 68% for **19** or 32% for **20**; (b) Methylamine, K_2CO_3, DMF, 130 °C, 16 h, 54% for **21** and 48% for **22**; (c) H_2, Pd/C, MeOH, 2 h, 78% for **23** and 85% for **24**; (d) **16**, EDC, HOAt, DMF; (e) AcOH, 130

°C, 0.5 h, 37% for **25** (over 2 steps) and 50% for **26** (over 2 steps); (f) Bis(pinacolato)diboron, $PdCl_2(dppf)\cdot CH_2Cl_2$, KOAc, dioxane, 120 °C, microwave; (g) **12**, $PdCl_2(dppf)\cdot CH_2Cl_2$, DME, 2 M Na_2CO_3 (aq), 120 °C, microwave; (h) 2-Bromo-*N*,*N*-dimethylisonicotinamide, $PdCl_2(dppf)\cdot CH_2Cl_2$, DME, 2 M Na_2CO_3 (aq), 120 °C, microwave; (i) TFA, CH_2Cl_2, 15% for **7** (over 2 steps) and 20% for **8** (over 2 steps), and 36% for **9** (over 3 steps).

For the synthesis of compounds **7–9** containing *N*-methyl and piperidinyl groups on benzimidazole ring, 1-bromo-2-fluoro-3-nitrobenzene was reacted with tert-butyl piperazine-1-carboxylate or tert-butyl (*S*)-2-methylpiperazine-1-carboxylate under a palladium-catalyzed amination reaction condition[59] (Scheme 3). The S_NAr amination reaction of **19** or **20** with methylamine followed by the reduction of the nitro group of **21** or **22** yielded bis-anilino intermediate **23** or **24**. The following amide bond formation/cyclization reactions with **16** provided the benzimidazole derivative **25** or **26**, which further underwent Suzuki coupling reaction with **12** to afford **7** or **8** after Boc-deprotection. Compound **26** was converted to the corresponding boronic ester **27**, and subsequent palladium-catalyzed cross coupling reaction with 2-bromo-*N*,*N*-dimethylisonicotinamide and the removal of Boc group led to compound **9**.

CONCLUSION

In summary, structure-based rational drug design utilizing a published MNK crystal structure allowed for the rapid development of a fragment hit to a potent and selective inhibitor of MNK1 and MNK2 kinases (**9**) which had good solubility and permeability. This compound exhibited superior potency and selectivity compared to MNK inhibitors described in the literature and can be used as a lead to further evaluate and prosecute this pathway and as a starting point for future drug discovery efforts.

EXPERIMENTAL SECTION

Chemistry. The compounds and/or intermediates were characterized by high performance liquid chromatography (HPLC) using a Waters Millenium chromatography system with a 2695 Separation Module (Milford, MA). The analytical columns were Alltima™ C18 reverse phase, 4.6 × 50 mm, flow 2.5 mL/min, from Alltech (Deerfield, IL). A gradient elution was used (flow 2.5 mL/min), typically starting with 5% acetonitrile/95% water and progressing to 100% acetonitrile over a period of 10 min. All solvents contained 0.1% TFA. Compounds were detected by ultraviolet light (UV) absorption at either 220 or 254 nm. HPLC solvents were from Burdick and Jackson (Muskegan, MI) or Fisher Scientific (Pittsburgh, PA). All compounds where biological data are presented have >95% purity as determined by HPLC. In some instances, purity was assessed by thin layer chromatography (TLC) using glass or plastic backed silica gel plates, such as, for example, Baker-Flex Silica Gel 1B2-F flexible sheets. TLC results were readily detected visually under ultraviolet light, or by employing well known iodine vapor and other various staining techniques.

Mass spectrometric analysis was performed on one of two LCMS instruments: a Waters System (Alliance HT HPLC and a Micromass ZQ mass spectrometer; Column: Eclipse XDB-C18, 2.1 × 50 mm; solvent system: 5-95% (or 35-95%, or 65-95% or 95-95%) acetonitrile in water with 0.05% TFA; flow rate 0.8 mL/min; molecular weight range 200-1500; cone Voltage 20 V; column temperature 40 °C) or a Hewlett Packard System (Series 1100 HPLC; Column: Eclipse XDB-C18, 2.1 × 50 mm; solvent system: 1-95% acetonitrile in water with 0.05% TFA; flow rate 0.8 mL/min; molecular weight range 150-850; cone Voltage 50 V; column temperature 30 °C). All masses were reported as those of the protonated parent ions.

HRMS ESI-MS data were recorded using a Synapt G2 HDMS (TOF mass spectrometer, Waters) with electrospray ionization source. The resolution of the MS system was approximately 15000. Leucine Enkephalin was used as lock mass (internal standard) infused from lockspray probe. The compound was infused into the mass spectrometer by UPLC (Acquity, Waters) from sample probe. The separation was performed on Acquity UPLC BEH-C18 1 × 50 mm column at 0.2 mL/min flow rate with the gradient from 5% to 95% in 3 min. Solvent A was water with 0.1% formic acid and solvent B was acetonitrile with 0.1% formic acid. The mass accuracy of the system has been found to be <5 ppm with lock mass.

^{1}H-Nuclear magnetic resonance (NMR) analysis was performed on some of the compounds with a Varian 300 or 400 MHz NMR and a Bruker 500 MHz NMR. The spectral reference was either TMS or the known chemical shift of the solvent. ^{13}C-NMR spectra were recorded using a Bruker AVANCE-500 NMR spectrometer operating at a frequency of 125.77 MHz for ^{13}C equipped with a 5 mm BBO probe.

Preparative separations were carried out using a Teledyne ISCO chromatography system, by flash column chromatography using silica gel (230-400 mesh) packing material, or by HPLC using a Waters 2767 Sample Manager, C18 reversed phase column, 30 × 50 mm, flow 75 mL/min. Typical solvents employed for the Teledyne ISCO chromatography system and flash column chromatography were dichloromethane, methanol, ethyl acetate, hexane, acetone, aqueous ammonia (or ammonium hydroxide), and triethylamine. Typical solvents employed for the reverse phase HPLC were varying concentrations of acetonitrile and water with 0.1% TFA.

3-(1H-Benzo[d]imidazol-2-yl)pyridin-2-amine (2).[60,61] To a solution of 3-(4,4,5,5-tetramethyl-1,3,2-dioxaborolan-2-yl)pyridin-2-amine (633 mg, 2.88 mmol) in DME (9 mL) and 2 M Na_2CO_3 (aq, 3.3 mL) in a microwave vial was added 2-bromo-1*H*-benzo[*d*]imidazole (436 mg, 2.2 mmol)

and $PdCl_2(dppf)\cdot CH_2Cl_2$ (126 mg, 160 μmol). The reaction was heated at 130 °C for 20 min under microwave irradiation. The reaction mixture was partitioned between EtOAc (30 mL) and water (30 mL). After the two layers were separated, the organic layer was washed with water and brine, dried over anhydrous Na_2SO_4, filtered, and concentrated in vacuo. The crude product was purified by automated flash chromatography (30-100% EtOAc in heptane) to yield **2** (144 mg, 31%). LCMS (m/z): 211 (MH^+), 0.46 min. HRMS (m/z) calcd for $C_{12}H_{11}N_4$ (MH^+) 211.0984, found 211.0981. HPLC: 2.35 min, >98% purity. ^{1}H NMR (400 MHz, CD_3OD) δ ppm 8.13 (dd, *J* = 7.83, 1.57 Hz, 1H), 8.03 (dd, *J* = 5.09, 1.57 Hz, 1H), 7.59 (br. s, 2H), 7.24 (dd, *J* = 5.87, 3.13 Hz, 2H), 6.77 (dd, *J* = 7.43, 5.09 Hz, 1H).

3-(1H-Benzo[d]imidazol-2-yl)-5-bromopyridin-2-amine (10). To a solution of **2** (132 mg, 0.63 mmol) in DMF (4 mL) was added NBS (112 mg, 0.63 mmol) at 0 °C. The reaction mixture was stirred at 0 °C for 20 min. After water (0.5 mL) was added, a precipitate formed and was filtered off. The residue was purified by preparative reverse phase HPLC. After the removal of acetonitrile from the combined pure fractions followed by addition of saturated Na_2CO_3 (aq), the product was extracted with EtOAc (200 mL). The organic layer was washed with water, filtered, and concentrated in vacuo to yield **10** (104 mg, 57%). LCMS (m/z): 288.9, 290.9 (MH^+), 0.55 min. ^{1}H NMR (400 MHz, CD_3OD) δ ppm 8.29 (d, *J* = 2.35 Hz, 1H), 8.08 (d, *J* = 1.96 Hz, 1H), 7.60 (br. s, 2H), 7.32-7.18 (m, 2H).

3-(1H-Benzo[d]imidazol-2-yl)-5-phenylpyridin-2-amine (3).[62] To **10** (20 mg, 0.069 mmol) in a microwave vial was added **11** (17.1 mg, 0.14 mmol), $PdCl_2(dppf)\cdot CH_2Cl_2$ (8.5 mg, 10.4 μmol), DME (800 μL), and 2 M Na_2CO_3 (aq, 140 μL). The reaction was heated at 130 °C for 15 min under microwave irradiation. The reaction mixture was partitioned between EtOAc (3 mL) and water (3 mL). After the two layers were separated, the organic layer was washed with water and

brine, dried over anhydrous Na_2SO_4, filtered, and concentrated in vacuo. The crude product was purified by preparative reverse phase HPLC. The pure fractions were combined and lyophilized to yield **3** as TFA salt (4.4 mg, 16%). LCMS (m/z): 287 (MH^+), 0.67 min. HRMS (m/z) calcd for $C_{18}H_{15}N_4$ (MH^+) 287.1297, found 287.1295. HPLC: 2.57 min, >99% purity. ^{1}H NMR (400 MHz, CD_3OD) δ ppm 8.98 (d, *J* = 1.96 Hz, 1H), 8.30 (d, *J* = 1.96 Hz, 1H), 7.79-7.74 (m, 2H), 7.70 (dd, *J* = 5.48, 3.52 Hz, 2H), 7.56 (t, *J* = 7.63 Hz, 2H), 7.51-7.42 (m, 1H), 7.40-7.32 (m, 2H).

3-(6-Amino-5-(1H-benzo[d]imidazol-2-yl)pyridin-3-yl)-N,N-dimethylbenzamide (4). To **10** (20 mg, 0.069 mmol) in a microwave vial was added **12** (26.7 mg, 0.14 mmol), $PdCl_2(dppf)\cdot CH_2Cl_2$ (8.5 mg, 10.4 μmol), DME (800 μL), and 2 M Na_2CO_3 (aq, 140 μL). The reaction was heated at 130 °C for 15 min under microwave irradiation. The reaction mixture was partitioned between EtOAc (3 mL) and water (3 mL). After the two layers were separated, the organic layer was washed with water and brine, dried over anhydrous Na_2SO_4, filtered, and concentrated in vacuo. The crude product was purified by preparative reverse phase HPLC. The pure fractions were combined and lyophilized to yield **4** as TFA salt (7 mg, 21%). LCMS (m/z): 358.1 (MH^+), 0.62 min. HRMS (m/z) calcd for $C_{21}H_{20}N_5O$ (MH^+) 358.1668, found 358.1667. HPLC: 1.17 min, >99% purity. ^{1}H NMR (400 MHz, CD_3OD) δ ppm 8.98 (d, *J* = 1.96 Hz, 1H), 8.36 (d, *J* = 1.96 Hz, 1H), 7.87 (d, *J* = 7.83 Hz, 1H), 7.82 (s, 1H), 7.71 (dd, *J* = 5.87, 3.52 Hz, 2H), 7.65 (t, *J* = 7.63 Hz, 1H), 7.53 (d, *J* = 7.83 Hz, 1H), 7.40-7.32 (m, 2H), 3.16 (s, 3H), 3.07 (s, 3H).

tert-Butyl 4-(3-amino-2-nitrophenyl)piperazine-1-carboxylate (13). To 3-chloro-2-nitroaniline (1 g, 5.8 mmol) in a microwave vial was added K_2CO_3 (2 g, 14.5 mmol), tert-butyl piperazine-1-carboxylate (2.7 g, 14.5 mmol), and DMF (18 mL) at room temperature. The reaction mixture was heated at 130 °C in oil bath for 28 h. After diluted with water, the reaction

mixture was extracted with EtOAc (100 mL) three times. The combined organic layers were washed with water and brine, dried over anhydrous Na_2SO_4, filtered, and concentrated in vacuo. The crude product was purified by automated flash chromatography (0-50% EtOAc in heptane) to yield **13** (890 mg, 48%). LCMS (m/z): 323 (MH^+), 0.87 min. ^{1}H NMR (400MHz, $CDCl_3$) δ ppm 7.15 (t, *J* = 8.0 Hz, 1H), 6.41 (d, *J* = 8.2 Hz, 1H), 6.45 (d, *J* = 8.2 Hz, 1H), 4.78 (br. s, 2 H), 3.58-3.48 (m, 4 H), 2.95 (br. s, 4 H), 1.48 (s, 9 H).

tert-Butyl 4-(2,3-diaminophenyl)piperazine-1-carboxylate (14). A solution of **13** (800 mg, 2.5 mmol) in MeOH (8.3 mL) was flushed with nitrogen gas for 10 min followed by addition of Pd/C (26 mg, 0.25 mmol). After charged with hydrogen gas, the reaction mixture was equipped with hydrogen gas balloon and stirred at room temperature for 1 h. The reaction mixture was filterd through diatomaceous earth and washed with MeOH (10 mL) and EtOAc (20 mL). The filtrate was concentrated in vacuo to yield **14** (700 mg, 96%) which was used in the next step without further purification. LCMS (m/z): 293 (MH^+), 0.6 min. ^{1}H NMR (400MHz, $CDCl_3$) δ ppm 6.79-6.67 (m, 1H), 6.63-6.55 (m, 2H), 3.72-3.42 (m, 4H), 3.22 (br. s, 2 H), 2.84 (br. s, 4H), 1.55-1.42 (m, 9H).

tert-Butyl 4-(2-(2-amino-5-bromopyridin-3-yl)-1H-benzo[d]imidazol-7-yl)piperazine-1-carboxylate (17). To a solution of 2-amino-5-bromonicotinic acid (**15**) (278 mg, 1.28 mmol) in acetonitrile (6 mL) was added **14** (375 mg, 1.28 mmol), HATU (683 mg, 1.8 mmol), and DIEA (0.43 mL, 2.4 mmol). The reaction mixture was stirred at room temperature for 6 h. LCMS indicated that the coupling reaction was completed. LCMS (m/z): 491, 493 (MH^+), 0.83 min. After partitioning between EtOAc (150 mL) and saturated $NaHCO_3$ (aq, 150 mL), the organic layer was washed with water and brine, dried over anhydrous Na_2SO_4, filtered off, and concentrated in vacuo. The crude product was dissolved in acetic acid (4 mL, 70 mmol). The

reaction mixture was heated at 120 °C in oil bath for 1 h. After neutralizing with 1 N NaOH (aq), the reaction mixture was extracted by EtOAc. The combined organic layers were washed with water and brine, dried over anhydrous Na_2SO_4, filtered, and concentrated in vacuo. The crude product was purified by automated flash chromatography to yield **17** (248 mg, 41%). LCMS (m/z): 473, 475 (MH^+), 0.81 min. ^{1}H NMR (400MHz, CD_3OD) δ ppm 8.29 (m, 1 H), 8.07 (d, *J* = 1.96 Hz, 1 H), 7.09-7.23 (m, 2 H), 6.70 (m, 1 H), 3.69 (m, 4 H), 3.45 (m, 4 H), 3.69 (s, 9 H).

3-(6-Amino-5-(7-(piperazin-1-yl)-1H-benzo[d]imidazol-2-yl)pyridin-3-yl)-N,N-dimethylbenzamide (5). To **17** (32 mg, 0.068 mmol) in a microwave vial was added **12** (26.1 mg, 0.135 mmol), DME (600 μL), 2 M Na_2CO_3 (aq, 135 μL), and $PdCl_2(dppf)\cdot CH_2Cl_2$ (8.29 mg, 10.1 μmol). The reaction mixture was heated at 120 °C for 15 min under microwave irradiation. The reaction mixture was partitioned between EtOAc (3 mL) and water (3 mL). After the two layers were separated, the organic layer was washed with water and brine, dried over anhydrous Na_2SO_4, filtered, and concentrated in vacuo. The crude product was dissolved in 2 mL of 4 M HCl in dioxane. The reaction mixture was stirred at room temperature for 1 h. After the reaction mixture was concentrated to dryness, the crude product was purified by preparative reverse phase HPLC. The pure fractions were combined and lyophilized to yield **5** as TFA salt (12.1 mg, 32%). LCMS (m/z): 457.1 (MH^+), 0.56 min. HRMS (m/z) calcd for $C_{25}H_{28}N_7O$ (MH^+) 442.2355, found 442.2349. HPLC: 1.92 min, >99% purity. ^{1}H NMR (400 MHz, CD_3OD) δ ppm 8.89 (d, *J* = 1.96 Hz, 1H), 8.36 (d, *J* = 1.96 Hz, 1H), 7.83 (d, *J* = 7.83 Hz, 1H), 7.78 (s, 1H), 7.62 (t, *J* = 7.63 Hz, 1H), 7.49 (d, *J* = 7.43 Hz, 1H), 7.26-7.30 (m, 2H), 6.77-6.84 (m, 1H), 3.71 (d, *J* = 5.09 Hz, 4H), 3.46-3.56 (m, 4H), 3.14 (s, 3H), 3.04 (s, 3H).

3-(5-Amino-6-(7-(piperazin-1-yl)-1H-benzo[d]imidazol-2-yl)pyrazin-2-yl)-N,N-dimethylbenzamide (6). Following the steps c, d, e, and f in Scheme 2, compounds **12**, **14** and

16 yielded **6** as TFA salt (8.2 mg, 20%). LCMS (m/z): 443.1 (MH^+), 0.62 min. HRMS (m/z) calcd for $C_{24}H_{27}N_8O$ (MH^+) 443.2308, found 443.2310. HPLC: 2.56 min, >99% purity. ^{1}H NMR (300 MHz, DMSO-d^6) δ ppm 8.83 (s, 1 H), 8.32 (d, J = 7.9 Hz, 1 H), 8.26 (s, 1 H), 7.55 (t, J = 7.6 Hz, 1 H), 7.37 (d, J = 7.3 Hz, 1 H), 7.29-7.17 (m, 2 H), 6.69 (d, J = 6.7 Hz, 1 H), 3.69 (br. s., 4 H), 3.39 (m , 4H) 3.03 (s, 3 H), 2.94 (s, 3 H).

tert-Butyl 4-(2-fluoro-3-nitrophenyl)piperazine-1-carboxylate (19). A solution of tert-butyl piperazine-1-carboxylate (1.9 g, 10.2 mmol), 1-bromo-2-fluoro-3-nitrobenzene (1.5 g, 6.8 mmol), cesium carbonate (4.4 g, 13.6 mmol), Xantphos (237 mg, 0.409 mmol), $Pd_2(dba)_3$ (312 mg, 0.34 mmol), and dioxane (23 mL) in a sealed glass reaction vessel was flushed with nitrogen gas for 10 min. Then, the reaction mixture was heated at 110 °C in oil bath overnight. After diluted with water, the reaction mixture was extracted with EtOAc (100 mL) three times. The combined organic layers were washed with water, saturated $NaHCO_3$ (aq), and brine. The organic layer was dried over anhydrous Na_2SO_4, filtered, and concentrated in vacuo. The crude product was purified by automated flash chromatography (0-40% EtOAc/heptane) to yield **19** (2.2 g, 68%). LCMS (m/z): 270 (MH^+-Boc), 1.15 min. ^{1}H NMR (400MHz, $CDCl_3$) δ ppm 7.59 (d, J = 3.5 Hz, 1H), 7.21-7.15 (m, 2H), 3.68-3.55 (m, 4H), 3.14- 3.05 (m, 4 H), 1.54-1.43 (m, 9H).

tert-Butyl 4-(2-(methylamino)-3-nitrophenyl)piperazine-1-carboxylate (21). To a solution of **19** (500 mg, 1.54 mmol) in DMF (3 mL) was added methylamine (2 M solution in THF; 1.5 mL, 3.07 mmol). The reaction mixture was stirred at 130 °C overnight. After quenched with saturated $NaHCO_3$ (aq), the reaction mixture was extracted with EtOAc (10 mL) three times. The combined organic layers were washed with water and brine, dried over anhydrous Na_2SO_4, filtered, and concentrated in vacuo. The crude product was purified by automated flash

chromatography (gradient EtOAc in heptane) to yield **21** (280 mg, 54%). R_f = 0.3 (30% EtOAc in heptane). LCMS (m/z): 337 (MH^+), 1.06 min. ^{1}H NMR (400MHz, $CDCl_3$) δ ppm 7.73 (dd, *J* = 1.2, 8.6 Hz, 1H), 7.15 (dd, *J* = 1.4, 7.6 Hz, 1H), 6.72 (t, *J* = 8.0 Hz, 1H), 3.69-3.52 (m, 4H), 3.00 (d, *J* = 3.9 Hz, 3H), 2.88 (br. s, 4H), 1.52-1.46 (m, 9H).

tert-Butyl 4-(3-amino-2-(methylamino)phenyl)piperazine-1-carboxylate (23). A solution of **21** (280 mg, 0.83 mmol) in MeOH (2.8 mL) was flushed with nitrogen gas for 10 min followed by addition of Pd/C (89 mg). After charged with hydrogen gas, the reaction mixture was equipped with hydrogen gas balloon and stirred at room temperature for 2 h. The reaction mixture was filterd through diatomaceous earth and washed with MeOH (5 mL) and EtOAc (10 mL). The filtrate was concentrated in vacuo to yield **23** (200 mg, 78%), which was used in the next step without further purification. LCMS (m/z): 307.1 (MH^+), 0.67 min.

tert-Butyl 4-(2-(3-amino-6-bromopyrazin-2-yl)-1-methyl-1H-benzo[d]imidazol-7-yl)piperazine-1-carboxylate (25). To a solution of **23** (253 mg, 0.826 mmol) in DMF (2.8 mL) was added **16** (180 mg, 0.11 mmol), HOAt (135 mg, 0.99 mmol), and EDC (206 mg, 1.07 mmol). The reaction mixture was stirred at room temperature overnight. LCMS indicated that the coupling reaction was completed. LCMS (m/z): 506, 508 (MH^+), 0.82 min and 0.86 min. The reaction mixture was partitioned between EtOAc (10 mL) and saturated $NaHCO_3$ (aq, 10 mL). After the two layers were separated, the organic layer was washed with water and brine, dried over anhydrous Na_2SO_4, filtered off, and concentrated in vacuo. The crude product was dissolved in acetic acid (2 mL). The reaction mixture was heated at 130 °C in oil bath for 20 min. After neutralizing with 1 N NaOH (aq), the reaction mixture was extracted by EtOAc. The combined organic layers were washed with water and brine, dried over anhydrous Na_2SO_4, filtered, and

concentrated in vacuo to yield **25** (150 mg, 37%) which was used in the next step without further purification. LCMS (m/z): 488, 490 (MH^+), 1.12 min.

3-(5-Amino-6-(1-methyl-7-(piperazin-1-yl)-1H-benzo[d]imidazol-2-yl)pyrazin-2-yl)-N,N-dimethylbenzamide (7). To **25** (75 mg, 0.154 mmol) in a microwave vial was added **12** (59.3 mg, 0.31 mmol), DME (384 μL), 2 M Na_2CO_3 (aq, 128 μL), and $PdCl_2(dppf)\cdot CH_2Cl_2$ (18.1 mg, 23 μmol). The reaction mixture was heated at 120 °C for 15 min under microwave irradiation. The reaction mixture was partitioned between EtOAc (3 mL) and water (3 mL). After the two layers were separated, the organic layer was washed with water and brine, dried over anhydrous Na_2SO_4, filtered, and concentrated in vacuo. The crude product was dissolved in DCM (1 mL) and TFA (0.3 mL). The reaction mixture was stirred at room temperature for 1 h. After the reaction mixture was concentrated to dryness, the crude product was purified by preparative reverse phase HPLC. The pure fractions were combined and lyophilized to yield **7** as TFA salt (35 mg, 40%). LCMS (m/z): 457.1 (MH^+), 0.56 min. HRMS (m/z) calcd for $C_{25}H_{29}N_8O$ (MH^+) 457.2464, found 457.2465. HPLC: 2.19 min, >99% purity. ^{1}H NMR (400 MHz, DMSO-d^6) δ ppm 8.79 (s, 1H), 8.11 (d, J = 7.8 Hz, 1H), 8.03 (s, 1H), 7.60-7.49 (m, 2H), 7.38 (d, J = 7.4 Hz, 1H), 7.24 (t, J = 7.8 Hz, 1H), 7.07 (d, J = 7.8 Hz, 1H), 4.58 (s, 3H), 3.00 (s, 3H), 2.95 (s, 3H).

(S)-tert-Butyl 4-(2-fluoro-3-nitrophenyl)-2-methylpiperazine-1-carboxylate (20). A solution of (S)-tert-butyl 2-methylpiperazine-1-carboxylate (546 mg, 2.73 mmol), 1-bromo-2-fluoro-3-nitrobenzene (400 mg, 1.82 mmol), cesium carbonate (1.18 g, 3.64 mmol), Xantphos (63.1 mg, 0.109 mmol), $Pd_2(dba)_3$ (83 mg, 0.091 mmol), and dioxane (6 mL) in a sealed glass reaction vessel was flushed with nitrogen gas for 10 min. Then, the reaction mixture was heated at 110 °C in oil bath overnight. After diluted with water, the reaction mixture was extracted with EtOAc (15 mL) three times. The combined organic layers were washed with water, saturated $NaHCO_3$

(aq), and brine. The organic layer was dried over anhydrous Na_2SO_4, filtered, and concentrated in vacuo. The crude product was purified by automated flash chromatography (0-40% EtOAc in heptane) to yield **20** (200 mg, 32%). LCMS (m/z): 240 (MH^+-Boc), 1.09 min. ^{1}H NMR (400MHz, $CDCl_3$) δ ppm 7.63-7.54 (m, 1H), 7.20-7.13 (m, 2H), 4.35 (br. s, 1H), 3.98 (d, *J* = 13.3 Hz, 1H), 3.35-3.22 (m, 4H), 2.93 (dd, *J* = 3.5, 11.7 Hz, 1H), 2.87-2.78 (m, 1H), 1.49 (s, 9H), 1.36 (d, *J* = 6.7 Hz, 3H).

(S)-tert-Butyl 2-methyl-4-(2-(methylamino)-3-nitrophenyl)-piperazine-1-carboxylate (22). To a solution of **20** (200 mg, 0.59 mmol) in DMF (2 mL) was added methylamine (2 M solution in THF; 0.59 mL, 1.8 mmol). The reaction mixture was stirred at 130 °C overnight. After quenched with saturated $NaHCO_3$ (aq), the reaction mixture was extracted with EtOAc (10 mL) three times. The combined organic layers were washed with water and brine, dried over anhydrous Na_2SO_4, filtered, and concentrated in vacuo. The crude product was purified by automated flash chromatography (gradient EtOAc in heptane) to yield **22** (99 mg, 48%). R_f = 0.3 (30% EtOAc in heptane). LCMS (m/z): 351 (MH^+), 1.11 min. ^{1}H NMR (400MHz, $CDCl_3$) δ ppm 7.69 (d, *J* = 8.6 Hz, 1H), 7.12 (d, *J* = 6.7 Hz, 1H), 6.72 (t, *J* = 8.2 Hz, 1H), 6.58 (br. s., 1H), 4.39 (m, 1H), 3.96 (d, *J* = 12.9 Hz, 1H), 3.37-3.23 (m, 1H), 3.13 (d, *J* = 10.2 Hz, 1H), 2.96 (d, *J* = 5.5 Hz, 3H), 2.92-2.85 (m, 2H), 2.65-2.47 (m, 1H), 1.49 (s, 9H), 1.36 (d, *J* = 6.7 Hz, 3H).

(S)-tert-Butyl 4-(3-amino-2-(methylamino)phenyl)-2-methylpiperazine-1-carboxylate (24). A solution of **22** (180 mg, 0.51 mmol) in MeOH (17 mL) was flushed with nitrogen gas for 10 min followed by addition of Pd/C (55 mg, 0.51 mmol). After charged with hydrogen gas, the reaction mixture was equipped with hydrogen gas balloon and stirred at room temperature for 1 h. The reaction mixture was filtered through diatomaceous earth and washed with MeOH (20 mL) and EtOAc (50 mL). The filtrate was concentrated in vacuo to yield **24** (138 mg, 85%)

which was used in the next step without further purification. LCMS (m/z): 321.1 (MH^+), 0.69 min.

(S)-tert-Butyl 4-(2-(3-amino-6-bromopyrazin-2-yl)-1-methyl-1H-benzo[d]imidazol-7-yl)-2-methylpiperazine-1-carboxylate (26). To a solution of **16** (23.8 mg, 0.11 mmol) in DMF (364 μL) was added **24** (35 mg, 0.11 mmol), HOAt (17.8 mg, 0.13 mmol), and EDC (27.2 mg, 0.14 mmol). The reaction mixture was stirred at room temperature overnight. LCMS indicated that the coupling reaction was completed. LCMS (m/z): 520, 522 (MH^+), 0.90 min. After partitioning between EtOAc (10 mL) and saturated $NaHCO_3$ (aq, 10 mL), a solid was filtered off which was the desired product. The filtrate was washed with water and brine, dried over anhydrous Na_2SO_4, filtered off, and concentrated in vacuo to yield the crude product. The combined products were dissolved in acetic acid (2 mL). The reaction mixture was heated at 110 °C in oil bath for 20 min. After neutralizing with 1 N NaOH (aq), the reaction mixture was extracted by EtOAc. The combined organic layers were washed with water and brine, dried over anhydrous Na_2SO_4, filtered, and concentrated in vacuo to yield **26** (27 mg, 50%) which was used in the next step without further purification. LCMS (m/z): 502, 504 (MH^+), 1.16 min.

(S)-3-(5-amino-6-(1-methyl-7-(3-methylpiperazin-1-yl)-1H-benzo[d]imidazol-2-yl)pyrazin-2-yl)-N,N-dimethylbenzamide (8). Following the steps g and i in Scheme 3, compound **12** and **26** yielded compound **8** as TFA salt (14.6 mg, 20% over 2 steps). LCMS (m/z): 471.2 (MH^+), 0.59 min. HRMS (m/z) calcd for $C_{26}H_{31}N_8O$ (MH^+) 471.2621, found 471.2616. HPLC: 2.26 min, >99% purity. ^{1}H NMR (400 MHz, DMSO-d^6) δ ppm 9.05 (br. s, 1H), 8.83 (s, 1H), 8.15 (d, J = 7.8 Hz, 1H), 8.08 (s, 1H), 7.63-7.53 (m, 2H), 7.42 (d, J = 7.4 Hz, 1H), 7.27 (t, J = 7.8 Hz, 1H), 7.12 (d, J = 7.8 Hz, 1H), 4.61 (s, 3H), 3.52-3.37 (m, 6H), 2.99 (s, 3H), 2.95 (s, 3H), 2.87-2.77 (m, 1H), 1.30 (d, J = 5.9 Hz, 3H).

tert-Butyl (S)-4-(2-(3-amino-6-(4,4,5,5-tetramethyl-1,3,2-dioxaborolan-2-yl)pyrazin-2-yl)-1-methyl-1H-benzo[d]imidazol-7-yl)-2-methylpiperazine-1-carboxylate (27). To a solution of **26** (44 mg, 0.088 mmol) in dioxane (146 μL) in a microwave vial was added 4,4,4',4',5,5,5',5'-octamethyl-2,2'-bi(1,3,2-dioxaborolane) (44.5 mg, 0.175 mmol), $PdCl_2(dppf)\cdot CH_2Cl_2$, (7.15 mg, 8.76 μmol), and KOAc (25.8 mg, 0.263 mmol). After flushed with nitrogen gas for 10 min, the reaction mixture was heated at 120 °C for 10 min under microwave irradiation. The reaction mixture was filtered through diatomaceous earth. After washed with EtOAc, the filtrate was concentrated in vacuo to yield **27** which was used in the next step without further purification. LCMS (m/z): 468 (MH^+), 0.8 min for the boronic acid of the desired product.

(S)-2-(5-Amino-6-(1-methyl-7-(3-methylpiperazin-1-yl)-1H-benzo[d]imidazol-2-yl)pyrazin-2-yl)-N,N-dimethylisonicotinamide (9). To a solution of **27** (40 mg, 0.073 mmol) in DME (182 μL) and 2 M Na_2CO_3 (aq, 61 μL) in a microwave vial was added 2-bromo-*N*,*N*-dimethylisonicotinamide (25.0 mg, 0.11 mmol) and $PdCl_2(dppf)\cdot CH_2Cl_2$ (8.9 mg, 10.9 μmol). The reaction mixture was heated at 120 °C for 10 min under microwave irradiation. The reaction mixture was partitioned between EtOAc (3 mL) and water (3 mL). After the two layers were separated, the organic layer was washed with water and brine, dried over anhydrous Na_2SO_4, filtered, and concentrated in vacuo. The crude product was dissolved in CH_2Cl_2 (1 mL) and TFA (0.3 mL). The reaction mixture was stirred at room temperature for 1 h. After diluted with toluene (2 mL), the reaction mixture was concentrated to dryness. The crude product was purified by preparative reverse phase HPLC. The pure fractions were combined and lyophilized to yield **9** as TFA salt (16.4 mg, 36% over 3 steps). LCMS (m/z): 472.2 (MH^+), 0.54 min. HRMS (m/z) calcd for $C_{25}H_{30}N_9O$ (MH^+) 472.2573, found 472.2570. HPLC: 1.84 min, >99% purity. ^1H NMR (500 MHz, DMSO-d^6) δ ppm 9.28 (br. s, 1H), 9.11 (s, 1H), 8.75 (dd, J = 4.9, 0.7 Hz, 1H),

8.17 (s, 1H), 7.60 (d, *J* = 7.8 Hz, 1H), 7.42 (dd, *J* = 4.9, 1.5 Hz, 1H), 7.29 (t, *J* = 7.9 Hz, 1H), 7.13 (d, *J* = 7.7 Hz, 1H), 4.60 (s, 3H), 3.66 (br. s, 1H), 3.49 (d, *J* = 13.2 Hz, 6H), 3.05 (s, 3H), 2.98 (s, 3H), 2.88-2.79 (m, 1H), 1.32 (d, *J* = 6.3 Hz, 3H). ^{13}C NMR (125.77 MHz, DMSO-d^6) δ ppm 167.9, 154.6, 154.6, 149.7, 149.1, 145.0, 142.5, 141.6, 138.7, 136.9, 129.1, 125.6, 123.1, 120.5, 117.3, 116.4, 116.0, 56.2, 50.8, 49.0, 43.0, 38.8, 35.1, 34.6, 15.8.

MNK1a HTRF Assay. Full length wild type MNK1a was generated in-house. The final total MNK1a concentration in the assay was 0.5 nM. Full length ERK2 (used for activating MNK1a) was purchased from Invitrogen, Cat # PV3595. The final total ERK2 concentration was 0.5 nM. The crebtide peptide substrate, biotin-SGSGKRREILSRRPSYR-NH_2, was a custom synthesis purchased from the Tufts University Core Facility. The final concentration of crebtide peptide substrate was 200 nM. The ATP substrate (Adenosine-5'-triphosphate) was purchased from Roche Diagnostics. The final concentration of ATP substrate was 200 μM. Europium (Eu)-anti-phospho-creb substrate antibody was purchased from CisBio. The final concentration of antibody was 0.23 nM. The homogeneous time resolved fluorescence (HTRF) detection reagent streptavidin-XL665 was purchased from CisBio. The final concentration of SA-XL665 was 50 nM. HTRF was used for detection. The biotinylated-crebtide peptide was phosphorylated by activated MNK1a using the ATP substrate. The biotinylated-crebtide peptide substrate was bound to the streptavidin-XL665. The Eu-antibody will bind to the phosphorylated form of the biotinylated-crebtide peptide substrate, bringing the Europium and XL665 into close proximity. When these reagents are in close proximity, the Europium is excited at 320 nm resulting in a resonance energy transfer to the XL665 which gives an emission signal at 665 nm. Assays were carried out in 50 mM Hepes, pH = 7.5, 5 mM $MgCl_2$, 0.05% bovine serum albumin, 0.01% Tween-20, 1 mM dithiolthreitol, 2.5% dimethyl sulfoxide. Stop and detection steps are combined

using 50 mM Hepes, pH = 7.5, 20 mM EDTA, 0.1% bovine serum albumin, 0.4 M KF. General protocol: To 5 μL of MNK1a/ERK2, 0.25 μL of test compound in dimethyl sulfoxide was added. Crebtide peptide and ATP are mixed. 5 μL of the crebtide peptide/ATP mix was added to start the reaction. The reaction was allowed to proceed for 2 h. 10 μL of Ab/streptavidin-XL665/Stop-detection buffer was added. Plates are incubated at room temperature overnight, in the dark, to allow for detection development before being read. The assay was run in a 384-well format using white polypropylene Greiner plates.

MNK2b HTRF Assay. Full length wild type MNK2b was purchased from Millipore, Cat #14-664-K. The final total MNK2b concentration in the assay was 1 nM. The crebtide peptide substrate, biotin-SGSGKRREILSRRPSYR-NH_2, was a custom synthesis purchased from the Tufts University Core Facility. The final concentration of crebtide peptide substrate was 200 nM. The ATP substrate (Adenosine-5'-triphosphate) was purchased from Roche Diagnostics. The final concentration of ATP substrate was 200 μM. Europium (Eu)-anti-phospho-creb substrate antibody was purchased from CisBio. The final concentration of antibody was 0.23 nM. The homogeneous time resolved fluorescence (HTRF) detection reagent streptavidin-XL665 was purchased from CisBio. The final concentration of SA-XL665 was 50 nM. HTRF is used for detection. The biotinylated-crebtide peptide was phosphorylated by activated MNK2b using the ATP substrate. The biotinylated-crebtide peptide substrate was bound to the streptavidin-XL665. The Eu-antibody will bind to the phosphorylated form of the biotinylated-crebtide peptide substrate, bringing the Europium and XL665 into close proximity. When these reagents are in close proximity, the Europium is excited at 320 nm resulting in a resonance energy transfer to the XL665 which gives an emission signal at 665 nm. Assays were carried out in 50 mM Hepes, pH = 7.5, 5 mM $MgCl_2$, 0.05% bovine serum albumin, 0.01% Tween-20, 1 mM dithiolthreitol,

2.5% dimethyl sulfoxide. Stop and detection steps were combined using 50 mM Hepes, pH = 7.5, 20 mM EDTA, 0.1% bovine serum albumin, 0.4 M KF. General protocol: To 5 μL of MNK2b, 0.25 μL of test compound in dimethyl sulfoxide was added. Crebtide peptide and ATP are mixed. 5 μL of the crebtide peptide/ATP mix was added to start the reaction. The reaction was allowed to proceed for 1 h. 10 μL of Ab/streptavidin-XL665/Stop-detection buffer was added. Plates were incubated at room temperature overnight, in the dark, to allow for detection development before being read. The assay was run in a 384-well format using white polypropylene Greiner plates.

Phospho-EIF4E Inhibition. A quantitative electrochemiluminescence (ECL) assay was developed to measure cellular levels of EIF4E protein phosphorylated at S209. This assay was built using ECL reagents from MesoScale Discovery (MSD, Rockville, MD). Specifically, KMS11-luc cell were seeded at 300,000 cells/well in Costar 96 well plates (Cat # 3603) and treated with compounds for 3 h at 37 °C, 5% CO_2. Cell lysates were generated using a 2× MSD lysis buffer (300 mM NaCl, 40 mM Tris, pH 7.5, 2 mM EDTA, 2 mM EGTA, 2% Triton X-100) which was directly added to the well. 75 μL of the cell lysate was added to blocked 96-well GAM ECL plates and incubated overnight at 4 °C on a plate shaker. The following day, plates were washed with 1× wash buffer followed by incubation at room temperature for 2 h with an anti-phospho-EIF4E antibody (Epitomics Cat # 2227-1) 1:200 dilution together with goat anti-rabbit sulfo-tag antibody at a 1:400 dilution. The plates underwent a final wash before addition of 1.5× MSD Read buffer and detection of the phospho-EIF4E signal in a MSD Sector 6000 plate reader. Although total EIF4E levels were not affected by inhibitor treatment, the phospho-EIF4E signal to total YB1 signal was normalized for EC_{50} calculations. The total EIF4E was detected through the same protocol described for phospho-eIF4E, but utilized a total EIF4E

antibody (R&D Systems Cat # MAB3228, 1 μg/μl) with a sulfo-tag goat anti-rabbit antibody (MSD; 0.5 μg/mL) for detection (KMS11-luc cells were generated at Novartis, CMCC # 12904).

MNK proliferation assay. Antiproliferative effects of MNK inhibitors were determined using the Promega CellTiter-Glo luminescent assay, which measured metabolically active cells. KMS11-luc cells were seeded at 2500 cells/well in Costar 96 well plates (Costar # 3603). Two hours post-seeding, the cells were treated with compounds, and then the plates were incubated at 37 °C, 5% CO_2 for 5 days. At the assay end-point, an equal volume of Promega CellTiter-Glo® was added to the entire 96 well plate. Plates were then sealed and placed on a plate shaker for 2 min, then were let to sit in the dark for an additional 10 min at room temperature. The luminescent signal of the plates was then recorded using the Trilux MicroBeta 2 instrument. EC_{50} values were determined with ActivityBase/Xlfit using the following equation: y = A + ((B-A)/(1+((C/x)^D))) where the x-axis is reported as concentration in μM and Y-axis is % inhibition (KMS11-luc cells were generated at Novartis, CMCC # 12904).

QM Conformational Energy Calculations. Conformational energy calculations were carried out with Jaguar, an *ab initio* quantum chemistry software program, marketed by Schrödinger Inc.[52,63] Each torsion angle was scanned with a 5 degree interval. Resulting conformations were minimized with Jaguar program. The lowest energy conformation was considered as the ground state conformation. In the energy minimization calculation, default basis set and theory were used (6-31G**/DFT).

ASSOCIATED CONTENT

Supporting Information. The LE and LipE values of compounds **2**–**9** for MNK1 and MNK2 kinases and the result of MNK2 kinase sequence blast search and alignment are in supporting information. This material is available free of charge via the Internet at http://pubs.acs.org.

AUTHOR INFORMATION

Corresponding Author

*Email: wooseok.han@novartis.com

ACKNOWLEDGMENT

The authors thank Alice Wang, Dahzi Tang, and Dr. Shengtian Yang for analytical chemistry support, and Colin Lorentzen and Kent Wong for in vitro DMPK support.

ABBREVIATIONS

EIF4E, eukaryotic translation initiation factor 4E; MNK, mitogen-activated protein (MAP) kinase-interacting kinase; SPRY2, sprouty 2; PSF, PTB-associated splicing factor; hnRNP A1, heterogenous nuclear ribonucleoprotein A1; cPLA2, cytosolic phospholipase A2; CDK, cyclin-dependent kinase; PIM, proto-oncogene proviral integration site for moloney murine leukemia virus kinase; FLT, fms-related tyrosine kinase; ROCK, rho-associated protein kinase; P-loop, phosphate-binding loop; LE, ligand efficiency; LipE, lipophilic efficiency; logD, log of the octanol-water distribution coefficient at pH 7.4 of ionized and unionized compound; BOC, tert-butoxycarbonyl; S_NAr, nucleophilic aromatic substitution; HTS, high-throughput screening;

CL_{int}, intrinsic clearance; ER_h, hepatic extraction ratio; DME, dimethoxyethane; HOAt, 1-hydroxy-7-azabenzotriazole; EDC, 1-ethyl-3-(3-dimethylaminopropyl)carbodiimide; TFA, trifluoroacetic acid.

REFERENCES

(1) Cargnello, M.; Roux, P. P. Activation and function of the MAPKs and their substrates, the MAPK-activated protein kinases. *Microbiol. Mol. Biol. Rev*. **2011**, *75*, 50–83.

(2) Wang, X.; Flynn, A.; Waskiewicz, A. J.; Webb, B. L.; Vries, R. G.; Baines, I. A.; Cooper, J. A.; Proud, C. G. The phosphorylation of eukaryotic initiation factor eIF4E in response to phorbol esters, cell stresses, and cytokines is mediated by distinct MAP kinase pathways. *J. Biol. Chem*. **1998**, *273*, 9373–9377.

(3) Dhillon, A. S.; Hagan, S.; Rath, O.; Kolch, W. MAP kinase signalling pathways in cancer. *Oncogene* **2007**, *26*, 3279–3290.

(4) Pelletier, J.; Graff, J.; Ruggero, D.; Sonenberg, N. Targeting the eIF4F translation initiation complex: A critical nexus for cancer development. *Cancer Res.* **2014**, *75*, 250–263.

(5) Gingras, A. C.; Raught, B.; Sonenberg, N. eIF4 initiation factors: Effectors of mRNA recruitment to ribosomes and regulators of translation. *Annu. Rev. Biochem*. **1999**, *68*, 913–963.

(6) Hiremath, L. S.; Webb, N. R.; Rhoads, R. E. Immunological detection of the messenger RNA cap-binding protein. *J. Biol. Chem*. **1985**, *260*, 7843–7849.

(7) Duncan, R.; Milburn, S. C.; Hershey, J. W. Regulated phosphorylation and low abundance of HeLa cell initiation factor eIF-4F suggest a role in translational control. Heat shock effects on eIF-4F. *J. Biol. Chem*. **1987**, *262*, 380–388.

(8) Bhat, M.; Robichaud, N.; Hulea, L.; Sonenberg, N.; Pelletier, J.; Topisirovic, I. Targeting the translation machinery in cancer. *Nat. Rev. Drug Discovery* **2015**, *14*, 261–278.

(9) Waskiewicz, A. J.; Flynn, A.; Proud, C. G. Cooper, J. A. Mitogen-activated protein kinases activate the serine/threonine kinases Mnk1 and Mnk2. *EMBO J*. **1997**, *16*, 1909–1920.

(10) Topisirovic, I.; Ruiz-Gutierrez, M.; Borden, K. L. Phosphorylation of the eukaryotic translation initiation factor eIF4E contributes to its transformation and mRNA transport activities. *Cancer Res*. **2004**, *64*, 8639–8642.

(11) Diab, S.; Kumarasiri, M.; Yu, M.; Teo, T.; Proud, C.; Milne, R.; Wang, S. MAP kinase-interacting kinases–emerging targets against cancer. *Chem. Biol. Rev.* **2014**, *21*, 441–452.

(12) Joshi, S.; Platanias, L. C. Mnk kinase pathway: Cellular functions and biological outcomes. *World J. Biol. Chem*. **2014**, *5*, 321–333.

(13) Wendel, H. G.; Silva, R. L.; Malina, A.; Mills, J. R.; Zhu, H.; Ueda, T. Watanabe-Fukunaga, R.; Fukunaga, R.; Teruya-Feldstein, J.; Pelletier, J.; Lowe, S. W. Dissecting eIF4E action in tumorigenesis. *Genes Dev*. **2007**, *21*, 3232–3237.

(14) Furic, L.; Rong. L.; Larsson, O.; Koumakpayi, I. H.; Yoshida, K.; Brueschke, A.; Petroulakis, E.; Robichaud, N.; Pollak, M.; Gaboury, L. A.; Pandolfi, P. P.; Saad, F.; Sonenberg, N. eIF4E phosphorylation promotes tumorigenesis and is associated with prostate cancer progression. *Proc. Natl. Acad. Sci. U.S.A*. **2010**, *107*, 14134–14139.

(15) Ueda, T.; Sasaki, M.; Elia, A. J.; Chio, I. I.; Hamada, K.; Fukunaga, R.; Mak, T. W. Combined deficiency for MAP kinase-interacting kinase 1 and 2 (Mnk1 and Mnk2) delays tumor development. *Proc. Natl. Acad. Sci. U.S.A*. **2010**, *107*, 13984–13990.

(16) Zhang, M.; Fu, W.; Prabhu, S.; Moore, J. C.; Ko, J.; Kim, J. W.; Druker, B. J.; Trapp, V.; Fruehauf, J.; Gram, H.; Fan, H. Y.; and Ong, S. T. Inhibition of polysome assembly enhances imatinib activity against chronic myelogenous leukemia and overcomes imatinib resistance. *Mol. Cell. Biol*. **2008**, *28*, 6496–6509.

(17) Marzec, M.; Liu, X.; Wysocka, M.; Rook, A.H.; Odum, N.; Wasik, M.A. Simultaneous inhibition of mTOR-containing complex 1 (mTORC1) and MNK induces apoptosis of cutaneous T-cell lymphoma (CTCL) cells. *PLoS ONE* **2011**, *6*, e24849.

(18) Shi, Y.; Frost, P.; Hoang, B.;Yang, Y.; Fukunaga, R.; Gera, J.; Lichtenstein, A. MNK kinases facilitate c-myc IRES activity in rapamycin-treated multiple myeloma cells. *Oncogene* **2013**, *32*, 190–197.

(19) Grzmil, M.; Huber, R. M.; Hess, D.; Frank, S.; Hynx, D.; Moncayo, G.; Klein, D.; Merlo, A.; Hemmings, B. A. MNK1 pathway activity maintains protein synthesis in rapalog-treated gliomas. *J. Clin. Invest*. **2014**, *124*, 742–754.

(20) Eckerdt, F.; Beauchamp, E.; Bell, J.; Iqbal, A.; Su, B.; Fukunaga, R.; Lulla, R. R.; Goldman, S.; Platanias, L. C. Regulatory effects of a Mnk2-eIF4E feedback loop during mTORC1 targeting of human medulloblastoma cells. *Oncotarget* **2014**, *5*, 8442–8451.

(21) Altman, J. K.; Glaser, H.; Sassano, A.; Joshi, S.; Ueda, T.; Watanabe-Fukunaga, R.; Fukunaga, R.; Tallman, M. S.; Platanias, L. C. Negative regulatory effects of Mnk kinases in the

generation of chemotherapy-induced antileukemic responses. *Mol. Pharmacol.* **2010**, *78*, 778–784.

(22) Wu, H.; Hu, C.; Wang, A.; Weisberg, E. L.; Chen, Y.; Yun, C-. H.; Wang, W.; Liu, Y.; Liu, X.; Tian, B.; Wang, J.; Zhao, Z.; Liang, Y.; Li, B.; Wang, L.; Wang, B.; Chen, C.; Buhrlage, S. J.; Qi, Z.; Zou, F.; Nonami, A.; Li, Y.; Fernandes, S. M.; Adamia, S.; Stone, R. M.; Galinsky, I. A.; Wang, X.; Yang, G.; Griffin, J. D.; Brown, J. R.; Eck, M. J.; Liu, J.; Gray, N. S.; Liu, Q. Discovery of a BTK/MNK dual inhibitor for lymphoma and leukemia. *Leukemia* **2016**, *30*, 173–181.

(23) Mbatia, H. W.; Ramalingam, S.; Ramamurthy, V. P.; Martin, M. S.; Kwegyir-Afful, A. K.; Njar, V. C. O. Novel C‑4 heteroaryl 13-cis-retinamide Mnk/AR degrading agents inhibit cell proliferation and migration and induce apoptosis in human breast and prostate cancer cells and suppress growth of MDA-MB-231 human breast and CWR22Rv1 human prostate tumor xenografts in mice. *J. Med. Chem.* **2015**, *58*, 1900−1914.

(24) Ramamurthy, V. P.; Ramalingam, S.; Gediya, L. K.; Kwegyir-Afful, A. K.; Njar, V. C. O. Simultaneous targeting of AR and MNK signaling pathways by novel retinamides induce profound antitumor and anti-invasive activities in human prostate cancer cell lines. *Oncotarget* **2015**, 6, 3195–3210.

(25) DaSilva, J.; Xu, L.; Kim, H. J.; Miller, W. T.; Bar-Sagi, D. Regulation of sprouty stability by Mnk1-dependent phosphorylation. *Mol. Cell Biol.* **2006**, *26*, 1898–1907.

(26) Sharma, B.; Joshi, S.; Sassano, A.; Majchrzak, B.; Kaur, S.; Aggarwal, P.; Nabet, B.; Bulic, M.; Stein, B. L.; McMahon, B.; Baker, D. P.; Fukunaga, R.; Altman, J. K.; Licht, J. D.;

Fish, E. N.; Platanias, L. C. Sprouty proteins are negative regulators of interferon (IFN) signaling and IFN-inducible biological responses. *J. Biol. Chem*. **2012**, *287*, 42352–42360.

(27) Buxadé, M.; Morrice, N.; Krebs, D. L.; Proud, C. G. The PSF.p54nrb complex is a novel Mnk substrate that binds the mRNA for tumor necrosis factor alpha. *J. Biol. Chem*. **2008**, *283*, 57–65.

(28) Ziaei, S.; Shimada, N.; Kucharavy, H.; Hubbard, K. MNK1 expression increases during cellular senescence and modulates the subcellular localization of hnRNP A1. *Exp. Cell Res*. **2012**, *318*, 500–508.

(29) Hefner, Y.; Borsch-Haubold, A.G.; Murakami, M.; Wilde, J. I.; Pasquet, S.; Schieltz, D.; Ghomashchi, F.; Yates, J. R.; Armstrong, C. G.; Paterson, A.; Cohen, P.; Fukunaga, R.; Hunter, T.; Kudo, I.; Watson, S. P.; Gelb, M. H. Serine 727 phosphorylation and activation of cytosolic phospholipase A2 by MNK1-related protein kinases. *J. Biol. Chem*. **2000**, *278*, 37542–37551.

(30) Proud, C. G. Mnks, eIF4E phosphorylation and cancer. *Biochim. Biophys. Acta, Gene Regul. Mech.*. **2015**, *1849*, 766–773.

(31) Ueda, T., Watanabe-Fukunaga, R., Fukuyama, H., Nagata, S., Fukunaga, R. Mnk2 and Mnk1 are essential for constitutive and inducible phosphorylation of eukaryotic initiation factor 4E but not for cell growth or development. *Mol. Cell Biol*. **2004**, *24*, 6539–6549.

(32) Hou, J.; Lam, F.; Proud, C.; Wang, S. Targeting Mnks for cancer therapy. *Oncotarget* **2012**, *3*, 118–131.

(33) Carroll, M.; Borden, K. L. B. The Oncogene eIF4E: Using biochemical insights to target cancer. *J. Interferon Cytokine Res*. **2013**, *33*, 227–238.

(34) Oyarzabal, J.; Zarich, N.; Albarran, M. I.; Palacios, I.; Urbano-Cuadrado, M.; Mateos, G.; Reymundo, I.; Rabal, O.; Salgado, A.; Corrionero, A.; Fominaya, J.; Pastor, J.; Bischoff, J. R. Discovery of mitogen-activated protein kinase-interacting kinase 1 inhibitors by a comprehensive fragment-oriented virtual screening approach. *J. Med. Chem*. **2010**, *53*, 6618–6628.

(35) Teo, T.; Yang, Y.; Yu, M.; Basnet, S. K.; Gillam, T.; Hou, J.; Lam, F.; Schmid, R.M.; Kumarasiri, M.; Diab, S.; Albrecht, H.; Sykes, M. J.; Wang, S. An integrated approach for discovery of highly potent and selective Mnk inhibitors: screening, synthesis and biological evaluations. *Eur. J. Org. Chem*. **2015**, *103*, 539–550.

(36) Webster, K. R.; Goel, V. K.; Hung, I. N. J.; Parker, G. S.; Staunton, J.; Neal, M.; Molter1, J.; Chiang, G. G.; Jessen, K. A.; Wegerski, C. J.; Sperry, S.; Huang, V.; Chen, J.; Thompson, P. A.; Appleman, J. R.; Webber, S. E.; Sprengeler, P. A.; Reich, S. H. eFT508, a potent and selective mitogen-activated protein kinase interacting kinase (MNK) 1 and 2 inhibitor, is efficacious in preclinical models of diffuse large B-cell lymphoma (DLBCL). In *57th American Society of Hematology Annual Meeting & Exposition*, Orlando, FL, Dec 5–8, 2015; American Society of Hematology: Washington, DC, 2015; Session 625.

(37) Knauf, U.; Tschopp, C.; Gram, H. Negative regulation of protein translation by mitogen-activated protein kinase-interacting kinases 1 and 2. *Mol. Cell. Biol*. **2001**, *21*, 5500–5511.

(38) Bain, J.; Plater, L.; Elliott, M.; Shpiro, N.; Hastie, C. J.; McLauchlan, H.; Klevernic, I.; Arthur, J. S. C.; Alessi, D. R.; Cohen, P. The selectivity of protein kinase inhibitors: a further update. *Biochem. J*. **2007**, *408*, 297–315.

(39) Diab, S.; Teo, T.; Kumarasiri, M.; Li, P.; Yu, M.; Lam, F.; Basnet, S. K. C.; Sykes, M. J.; Albrecht, H.; Milne, R.; Wang, S. Discovery of 5-(2-(phenylamino)pyrimidin-4-yl)thiazol-2(3*H*)-one derivatives as potent Mnk2 inhibitors: synthesis, SAR analysis and biological evaluation. *ChemMedChem*. **2014**, *9*, 962–972.

(40) Konicek, B. W.; Stephens, J. R.; McNulty, A. M.; Robichaud, N.; Peery, R. B.; Dumstorf, C. A.; Dowless, M. S.; Iversen, P. W.; Parsons, S.; Ellis, K. E.; McCann, D. J.; Pelletier, J.; Furic, L.; Yingling, J. M.; Stancato, L. F.; Sonenberg, N.; Graff, J. R. Therapeutic inhibition of MAP kinase interacting kinase blocks eukaryotic initiation factor 4E phosphorylation and suppresses outgrowth of experimental lung metastases. *Cancer Res*. **2011**, *71*, 1849–1857.

(41) Altman, J. K.; Szilard, A.; Konicek, B. W.; Iversen, P. W.; Kroczynska, B; Glaser, H.; Sassano, A.; Vakana, E.; Graff, J. R.; Platanias, L.C. Inhibition of Mnk kinase activity by cercosporamide and suppressive effects on acute myeloid leukemia precursors. *Blood* **2013**, *121*, 3675–3681.

(42) Sussman, A.; Huss, K.; Chio, L-. C.; Elliott, M.; Shpiro, N.; Hastie, C. J.; Mclauchlan, H.; Klevernic, I.; Arthur, J. S. C.; Alessi, D. R.; Cohen, P. Discovery of cercosporamide, a known antifungal natural product, as a selective Pkc1 kinase inhibitor through high-throughput screening. *Eukaryotic Cell* **2004**, *3*, 932–943.

(43) 17 kinases are listed in the supporting information (Table 4).

(44) Reynolds, C. H.; Bembenek, S. D.; Tounge, B. A. The role of molecular size in ligand efficiency. *Bioorg. Med. Chem. Lett*. **2007**, *17*, 4258–4261; See supporting information for details (Table 3).

(45) Jauch, R.; Cho, M. K.; Jäkel, S.; Netter, C.; Schreiter, K.; Aicher, B.; Zweckstetter, M.; Jäckle, H.; Wahl, M. C. Mitogen-activated protein kinases interacting kinases are autoinhibited by a reprogrammed activation segment. *EMBO J*. **2006**, *25*, 4020–4032.

(46) Bissantz, C.; Kuhn, B.; Stahl, M. A medicinal chemist's guide to molecular interactions. *J. Med. Chem*. **2010**, *53*, 5061–5084.

(47) Kannan, S.; Poulsen, A.; Yang, H. Y.; Ho, M.; Ang, S. H.; Eldwin, T. S. W.; Jeyaraj, D. A.; Chennamaneni, L. R.; Liu, B.; Hill, J.; Verma, C. S.; Nacro, K. Probing the binding mechanism of Mnk inhibitors by docking and molecular dynamics simulations. *Biochemistry* **2015**, *54*, 32−46.

(48) Leeson, P. D.; Springthorpe, B. The influence of drug-like concepts on decision-making in medicinal chemistry. *Nat. Rev. Drug Discovery* **2007**, *6*, 881−890; See supporting information for the LE and LipE values of compounds **2**–**9** (Table 3).

(49) Shultz, M. D. The thermodynamic basis for the use of lipophilic efficiency (LipE) in enthalpic optimizations. *Bioorg. Med. Chem. Lett*. **2013**, *23*, 5992−6000.

(50) Compound **5** has moderate permeability (P_{app}A-B: 4.0×10^{-6} cm/s) with efflux ratio of 3.6 in Caco-2 permeability assay.

(51) Unpublished results.

(52) Bochevarov, A. D.; Harder, E.; Hughes, T. F.; Greenwood, J. R.; Braden, D. A.; Philipp, D. M.; Rinaldo, D.; Halls, M. D.; Zhang, J.; Friesner, R. A. Jaguar: A high-performance quantum chemistry software program with strengths in life and materials sciences. *Int. J. Quantum Chem*. **2013**, *113*, 2110–2142; See experimental section for details.

(53) The resulting torsion angle between the aminopyrazine and benzimidazole rings of compound **7** was 12 degrees.

(54) Leung, C. S.; Leung, S. S. F.; Tirado-Rives, J.; Jorgensen, W. L. Methyl effects on protein-ligand binding. *J. Med. Chem*. **2012**, *55*, 4489–4500.

(55) Compounds **6** and **7**: 3- to 7-fold decrease in the selectivity against CDK1 and CDK2 and 20- to 40-fold improvement in MNK1 and MNK2 potency.

(56) Taylor, R. Life science applications of the Cambridge Structural Database. *Acta Crystallogr.* **2002**, *D58*, 879–888.

(57) Recently, it was reported that CDK9 inhibition leads to the downregulation of MNK[35]. CDK9 IC_{50} for compound **9** was >25 μM.

(58) KMS11-luc proliferation EC_{50} for cercosporamide was >10 μM.

(59) Muci, A. R.; Buchwald, S. L. Practical palladium catalysts for C-N and C-O bond formation. *Topics in Curr. Chem*. **2002**, *219*, 131–209.

(60) Nunes, J.; Milne, J.; Bemis, J.; Xie, R.; Vu, C. B. ; Ng, P. Y.; Disch, J. S. Benzimidazole derivatives as sirtuin modulators. WO 2007019416 A1 2007.

(61) Harbeson, S. L.; Arnost, M. J.; Green, J.; Savic, V. Heteroaryl compounds useful as inhibitors of GSK-3. WO 2003066629 A2 2003.

(62) Drewry, D. H.; Hunter, R. N. III. Chemical compounds. WO 2004069160 A2 2004.

(63) Schrödinger Release 2014-1: *Jaguar*, version 8.3, Schrödinger, LLC, New York, NY, 2014.

Table of Contents graphic.